Available on CMS information server

CMS CR -2019/198

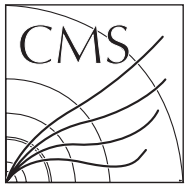

The Compact Muon Solenoid Experiment

Conference Report

Mailing address: CMS CERN, CH-1211 GENEVA 23, Switzerland

09 October 2019 (v5, 24 October 2019)

Higgs boson mass measurement using $\mathrm{H} \to \mathrm{ZZ} \to 4\ell$ decays at CMS

Jake Rosenzweig on behalf of the CMS Collaboration

Abstract

A summary of the methods used to make a precision measurement of the Higgs boson mass is presented. The final mass value for the Higgs boson is measured to be $m_{\mathrm{H}} = 125.26 \pm 0.21$ GeV. This analysis considers the $\mathrm{H} \to \mathrm{ZZ} \to 4\ell$ channel ($\ell = e, \mu$), using proton-proton collision data collected in 2016 corresponding to an integrated luminosity of 35.9 fb^{-1} at $\sqrt{s} = 13$ TeV by the CMS experiment at the LHC. A mass constraint is imposed on the invariant mass of the two leptons coming from the mostly on-shell Z boson to refit the lepton momenta and, hence, improve the measurement of the Higgs boson mass, per-event. The mass of the Higgs boson is extracted using a three-dimensional likelihood fit, which uses three observables per-event: (1) the refitted four-lepton invariant mass ($m'_{4\ell}$), (2) the refitted four-lepton mass uncertainty ($\mathcal{D}'_{\mathrm{mass}}$), and (3) a matrix element-based kinematic discriminant ($\mathcal{D}^{\mathrm{kin}}_{\mathrm{bkg}}$).

Presented at *DPF2019 2019 Meeting of the Division of Particles and Fields of the American Physical Society*

Higgs boson mass measurement using $\mathrm{H} \to \mathrm{ZZ} \to 4\ell$ decays at CMS

Jake Rosenzweig on behalf of the CMS Collaboration

Department of Physics
University of Florida, Gainesville, FL, USA

Abstract: A summary of the methods used to make a precision measurement of the Higgs boson mass is presented. The final mass value for the Higgs boson is measured to be $m_{\mathrm{H}} = 125.26 \pm 0.21$ GeV. This analysis considers the $\mathrm{H} \to \mathrm{ZZ} \to 4\ell$ channel ($\ell = e, \mu$), using proton-proton collision data collected in 2016 corresponding to an integrated luminosity of 35.9 fb^{-1} at $\sqrt{s} = 13$ TeV by the CMS experiment at the LHC. A mass constraint is imposed on the invariant mass of the two leptons coming from the mostly on-shell Z boson to refit the lepton momenta and, hence, improve the measurement of the Higgs boson mass, per-event. The mass of the Higgs boson is extracted using a three-dimensional likelihood fit, which uses three observables per-event: (1) the refitted four-lepton invariant mass ($m'_{4\ell}$), (2) the refitted four-lepton mass uncertainty ($\mathcal{D}'_{\mathrm{mass}}$), and (3) a matrix element-based kinematic discriminant ($\mathcal{D}^{\mathrm{kin}}_{\mathrm{bkg}}$).

Talk presented at the 2019 Meeting of the Division of Particles and Fields of the American Physical Society (DPF2019), July 29–August 2, 2019, Northeastern University, Boston, C1907293.

1 Introduction

In 2015, two major particle physics collaborations, CMS and ATLAS, jointly published measurements on the mass of the recently-discovered Higgs boson [1, 2]. These results used proton-proton collision data delivered by the LHC at a center-of-mass energy of 13 TeV during Run 1 (2011 and 2012) corresponding to a total integrated luminosity of approximately 25 fb^{-1} per collaboration. The Higgs boson mass (m_{H}) measurement during Run 1 using the combined results from both collaborations was $m_{\mathrm{H}} = 125.09 \pm 0.24$ GeV. Two Higgs boson decay channels were analyzed to obtain the final mass result: (1) $\mathrm{H} \to \gamma\gamma$ and (2) $\mathrm{H} \to \mathrm{ZZ} \to 4\ell$ (where $\ell = e, \mu$). The individual mass measurements for each decay channel, including statistical and systematic uncertainties, and their combined results per collaboration, are given in Table 1 [3].

In 2017, the precision on the aforementioned Run 1 mass measurement was superseded by CMS by considering only the $\mathrm{H} \to \mathrm{ZZ} \to 4\ell$ channel and using 2016 Run 2 data, corresponding to a total integrated luminosity of 35.9 fb^{-1}. The best value of m_{H} is determined by minimizing a three-dimensional (3D) likelihood fit of the following three observables: (1) the refitted four-lepton invariant mass ($m'_{4\ell}$), (2) the refitted four-lepton mass uncertainty ($\mathcal{D}'_{\mathrm{mass}}$), and (3) a matrix element-based kinematic discriminant ($\mathcal{D}^{\mathrm{kin}}_{\mathrm{bkg}}$). Each observable is evaluated on a per-event basis and uses refitted lepton transverse momenta (p_{T}) by performing a mass constraint on the more on-shell Z boson, which ultimately improves the precision of the 3D likelihood fit.

The Higgs boson mass resonance in the four-lepton state enables a precision measurement of m_{H} due to a large signal-to-background ratio and because of its intrinsically narrow width. The background processes consist of two kinds: (1) irreducible $\mathrm{q\bar{q}}/\mathrm{gg} \to \mathrm{ZZ}, \mathrm{Z}\gamma^*$ processes which skip Higgs boson production altogether, and (2) reducible $\mathrm{Z} + \mathrm{X}$, in which a Higgs boson decays into a Z boson and X, where X is typically a heavy flavor jet which decays into secondary leptons. These leptons are misidentified as prompt leptons and therefore this process is considered background. This $\mathrm{Z} + \mathrm{X}$ region is estimated using data-driven methods.

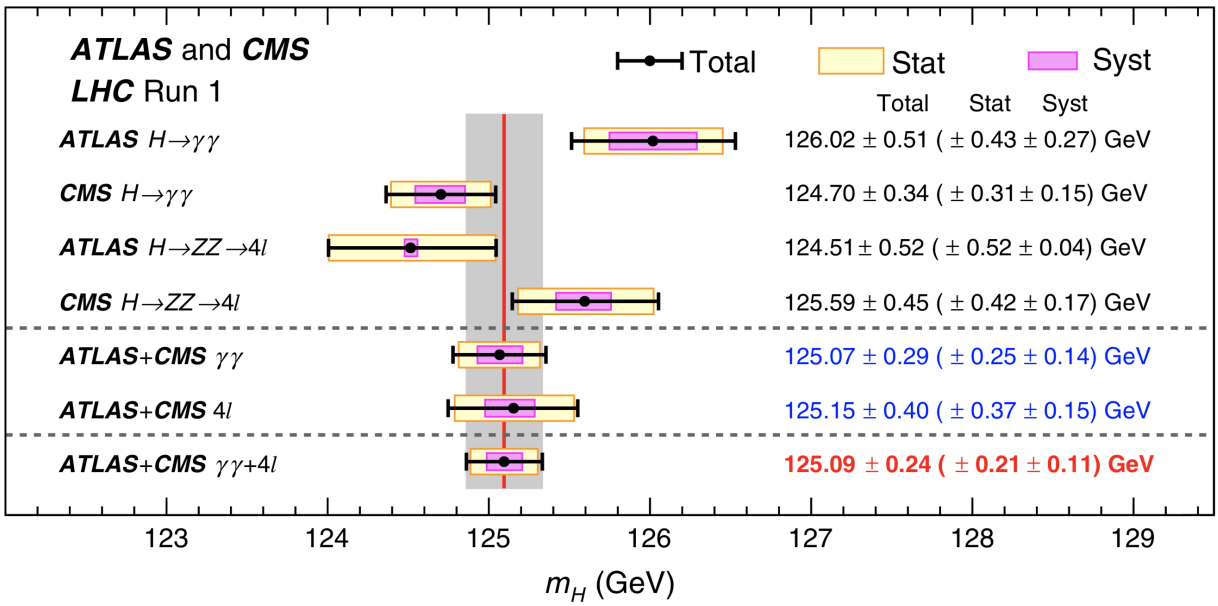

Table 1: The Higgs boson mass measurement results from the ATLAS and CMS Collaborations during the LHC Run 1 using two different decay channels in combination. The statistical (yellow bands), systematic (pink bands), and total (black bars) uncertainties are shown. The central value (red line) and the corresponding total uncertainty (gray bar) for the final combined mass measurement are shown at the bottom in red text [3].

2 Observables

Three observables are used to extract the Higgs boson mass using a three-dimensional likelihood fit that scans over m_{H}. Each observable is defined in the following subsections. The observables are:

1. the refitted four-lepton invariant mass ($m'_{4\ell}$),
2. the refitted four-lepton mass uncertainty on an event-by-event basis ($\mathcal{D}'_{\mathrm{mass}}$),
3. a matrix element-based kinematic discriminant ($\mathcal{D}^{\mathrm{kin}}_{\mathrm{bkg}}$).

It should be noted that an observable with a prime symbol ($'$) indicates that it has been updated using the refitted lepton p_{T} values as described in Section 3.

2.1 First Observable: Four-Lepton Invariant Mass $\left(m'_{4\ell}\right)$

The topology of the H $\rightarrow$ ZZ $\rightarrow 4\ell$ process is shown in Figure 1 (Left). A Higgs boson decays into two Z bosons, one of which is mostly on-shell (Z_1), while the other Z boson is mostly off-shell, Z_2. Each Z boson decays to opposite-sign, same-flavor leptons, $\mathrm{Z} \rightarrow \ell^-\ell^+$ ($\ell = e, \mu$), which yields the following final states: 4e, 4μ, and $2\mathrm{e}2\mu$. For each final state category, the four-lepton invariant mass ($m_{4\ell}$), is evaluated per-event. The distribution of $m_{4\ell}$ is shown in Fig. 1 (Right) [4]. The $m_{4\ell}$ observable gets updated to $m'_{4\ell}$ by a kinematic refitting of the lepton p_{T} values using a Z_1 mass constraint as described in Section 3.

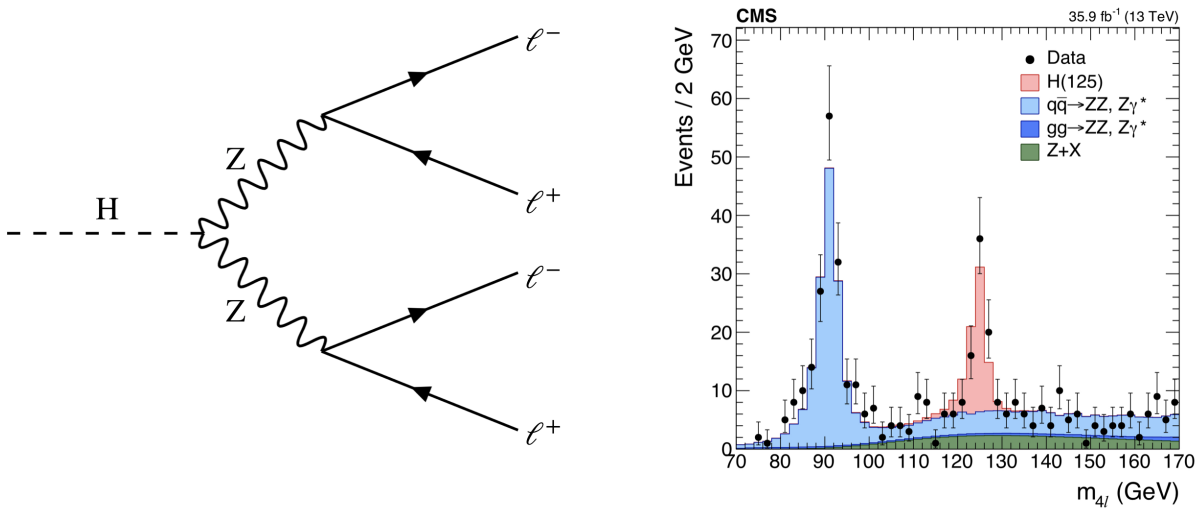

Figure 1: (Left) The Feynman diagram representing the $\mathrm{H} \to \mathrm{ZZ} \to 4\ell$ process. (Right) The four-lepton invariant mass distribution. The Higgs boson mass resonance (salmon color) stands well above the $\mathrm{q\bar{q}} \to \mathrm{ZZ}, \mathrm{Z}\gamma^*$ (light-blue), $\mathrm{gg} \to \mathrm{ZZ}, \mathrm{Z}\gamma^*$ (dark-blue), and $\mathrm{Z}+\mathrm{X}$ (green) background processes [4].

2.2 Second Observable: Relative Mass Uncertainty $\left(\mathcal{D}'_{\mathrm{mass}}\right)$

Per-event, the evaluation of $m_{4\ell}$ comes with an associated uncertainty ($\delta m_{4\ell}$) which is a function of the transverse momenta (p_{T,ℓ_k}) and the corresponding uncertainties ($\delta p_{\mathrm{T},\ell_k}$) of the four outgoing leptons:

$$\delta m_{4\ell} = F\Big(\{p_{T,\ell_1}, \delta p_{T,\ell_1}\}, \cdots, \{p_{T,\ell_4}, \delta p_{T,\ell_4}\}\Big). \tag{1}$$

This value is obtained via an error propagation technique which smears p_{T,ℓ_k} by its corresponding $\delta p_{\mathrm{T},\ell_k}$, lepton-by-lepton:

$$p_{\mathrm{T},k} \to p_{\mathrm{T},k} + \delta p_{\mathrm{T},k} = p'_{\mathrm{T},\ell_k} \tag{2}$$

where p'_{T,ℓ_k} is the smeared transverse momentum of lepton k. An increased precision on the measurement of p_{T,ℓ_k} (decreased $\delta p_{\mathrm{T},\ell_k}$) leads to an increased precision on $m_{4\ell}$ (decreased $\delta m_{4\ell}$). The $\delta p_{\mathrm{T},\ell_k}$ values are corrected to minimize $\delta m_{4\ell}$ using lepton p_{T} error correction factors (λ):

$$\delta p^{\mathrm{corr}}_{\mathrm{T},\ell_k} = \lambda \times \delta p_{\mathrm{T},\ell_k} \tag{3}$$

These λ values are evaluated by simulating $\mathrm{Z} \to \ell^-\ell^+$ ($\ell = e, \mu$) events and by extracting the resolution (σ) of the Z mass resonance from the $m_{\ell\ell}$ distribution. This mass distribution is fit using a Breit-Wigner probability density function (pdf) convoluted with a Crystal Ball (CB) pdf and a decaying exponential pdf. The fit then extracts the relevant parameters for each pdf, holds all of them fixed, except the resolution of the CB pdf (σ_{CB}) which gets replaced by:

$$\sigma_{\mathrm{CB}} \to \lambda \times \delta m_{\ell\ell}$$

where λ is the sought-after correction factor to be used in Eq. 3. A second fit, which is conditional on the per-event uncertainty of the dilepton invariant mass ($\delta m_{\ell\ell}$), finds the single, optimal λ value for this simulated sample of $\mathrm{Z} \to \ell^-\ell^+$ events.

It is important to note that, since different parts of the CMS detector have different lepton p_{T} resolutions, it is necessary to categorize each dilepton events into a specific kinematic bin, depending

on the pseudorapidity (η) and relative p_{T} uncertainties ($\delta p_{\mathrm{T}}/p_{\mathrm{T}}$) of the leptons detected by the various sub-detector regions [5]. Therefore, a λ correction factor is evaluated for each kinematic bin and subsequently used to correct the lepton transverse momentum uncertainty in the corresponding region, per Eq. 3. A closure test is performed to verify that the λ values are performing as intended. As shown in Fig. 2 [4], the measured relative mass uncertainties of the dilepton events within a specific kinematic bin agree with the predicted values. The $\delta p^{\mathrm{corr}}_{\mathrm{T},\ell_k}$ values are obtained per-event using Eq. 3. Next, each p'_{T,ℓ_k} is individually updated using Eq. 2. Finally, the total $\delta m_{4\ell}$ is evaluated using the updated p'_{T,ℓ_k} values per-event using Eq. 1.

It is useful to normalize $\delta m_{4\ell}$ with the corresponding $m_{4\ell}$ value and define the per-event relative mass uncertainty ($\mathcal{D}_{\mathrm{mass}}$) as:

$$\mathcal{D}_{\mathrm{mass}} = \frac{\delta m_{4\ell}}{m_{4\ell}.}$$

As will be described in Section 3, the $\mathcal{D}_{\mathrm{mass}}$ gets updated using refitted lepton p_{T} values and is promoted to a refitted, per-event relative mass uncertainty ($\mathcal{D}'_{\mathrm{mass}}$).

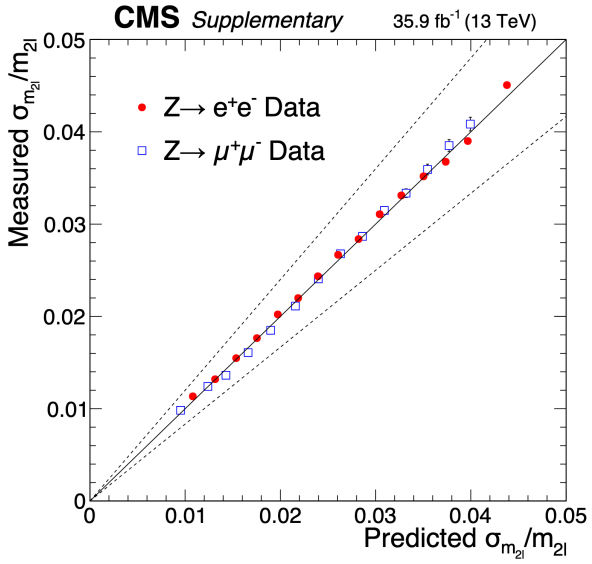

Figure 2: A closure test is used to validate the lepton p_{T} error correction values (λ). The measured relative mass uncertainty values (Measured $\sigma_{\mathrm{m}_{2\ell}}/m_{2\ell}$) for simulated $\mathrm{Z} \to \ell^-\ell^+$ events are compared with the predicted relative mass uncertainty values. Events are binned according to their predicted relative mass uncertainty such that approximately an equal number of events is found in each bin. Validation of the λ values is confirmed in each bin, for both final states (red dots for $2e$, open squares for 2μ), since the measured values are tightly bound around the 1-to-1 line (solid black). The dashed lines represent a 20% systematic uncertainty on the resolution during Run 1 [4].

2.3 Third Observable: Kinematic Discriminant $\left(\mathcal{D}^{\mathrm{kin}}_{\mathrm{bkg}}\right)$

Each Higgs boson decay event, whether signal or background, carries certain kinematical information about the particles involved, *e.g.*, the spins, momenta, and decay angles, of each particle. Fig. 3 (Left) shows an example of such a Higgs boson decay and the associated kinematical variables involved [4]. All the decay observables are then incorporated into a single variable ($\vec{\Omega}^{\mathrm{H}\to 4\ell}$) [6–8].

Then, a kinematic discriminant ($\mathcal{D}^{\rm kin}_{\rm bkg}$) can be constructed from $\vec{\Omega}^{\rm H\to 4\ell}$ to better discriminate between signal and background events. The $\mathcal{D}^{\rm kin}_{\rm bkg}$ is defined as:

$$\mathcal{D}^{\rm kin}_{\rm bkg} = \left[1 + \frac{P^{\rm q\bar{q}}_{\rm bkg}(\vec{\Omega}^{\rm H\to 4\ell}|m_{4\ell})}{P^{\rm gg}_{\rm sig}(\vec{\Omega}^{\rm H\to 4\ell}|m_{4\ell})}\right]^{-1} \tag{4}$$

where $P^{\rm q\bar{q}}_{\rm bkg}$ represents the probability density that an event is consistent with a $\rm q\bar{q} \to ZZ, Z\gamma^*$ background event, while $P^{\rm gg}_{\rm sig}$ represents the probability density that an event is consistent with a signal event. Fig. 3 (Right) [4] shows the three observables per-event, for simulation and data.

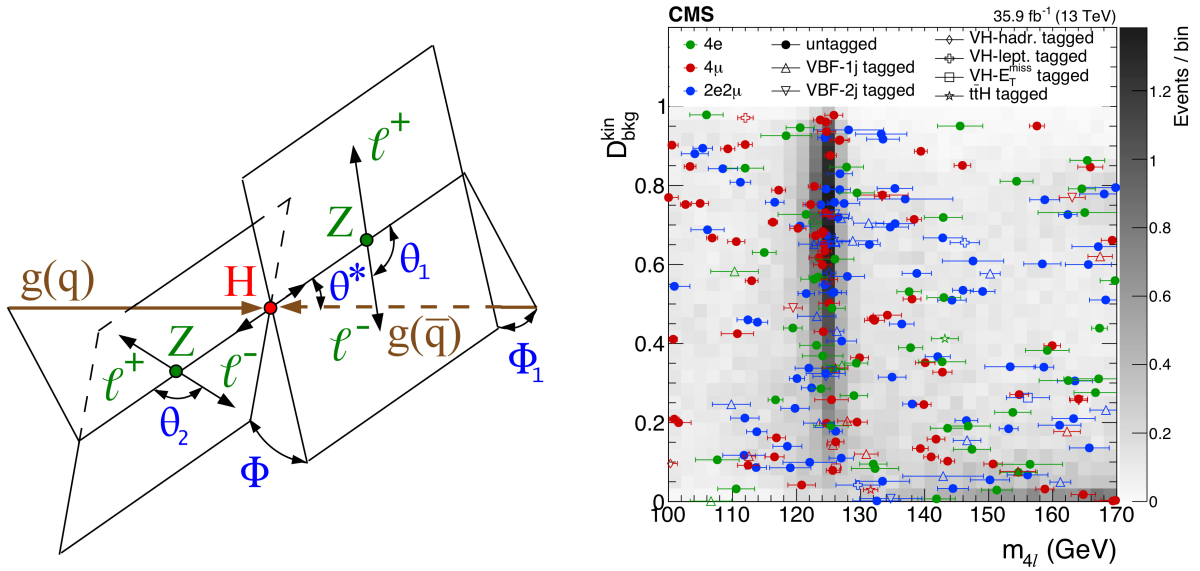

Figure 3: (Left) A $\rm gg(q\bar{q}) \to H \to ZZ \to 4\ell$ event, which shows the angular kinematical variables that go into $\vec{\Omega}^{\rm H\to 4\ell}$ and are then used to evaluate $\mathcal{D}^{\rm kin}_{\rm bkg}$, per-event [9]. (Right) The $\mathcal{D}^{\rm kin}_{\rm bkg}$ vs. $m_{4\ell}$ is plotted in the range $100 < m_{4\ell} < 170$ GeV, using $\mathcal{D}_{\rm mass}$ as the relative mass uncertainty on each data point. The expected number of Higgs boson decay events (dark gray region near 125 GeV) agrees relatively well with the observed data (green, red, and blue points for each type of final state) [4].

3 Kinematic Refit Using a $\rm Z_1$ Mass Constraint

The Higgs boson mass measurement can achieve even better precision by using knowledge of the mass and line shape of the mass resonance of the more on-shell Z boson ($\rm Z_1$). As shown in Fig. 4 (Left) the $\rm Z_1$ is mostly on-shell and therefore allows for precise fitting of its line shape, whereas the $\rm Z_2$ is mostly off-shell [4]. Because of the well-defined line shape of the $\rm Z_1$ mass resonance, and the fact that the narrow width of the resonance is similar to that of the detector resolution, a mass constraint is applied which allows for a refitting of the dilepton $p_{\rm T}$ values originating from the $\rm Z_1$, on a per-event basis. The mass constraint is used in maximizing the likelihood of the refitted lepton $p_{\rm T}$ values:

$$\mathcal{L}(\hat{p}^1_{\rm T}, \hat{p}^2_{\rm T}|p^1_{\rm T}, p^2_{\rm T}, \delta p^1_{\rm T}, \delta p^2_{\rm T}) = {\rm Gauss}(p^1_{\rm T}|\hat{p}^1_{\rm T}, \delta p^1_{\rm T}){\rm Gauss}(p^2_{\rm T}|\hat{p}^2_{\rm T}, \delta p^2_{\rm T})\mathcal{L}(m_{12}|m_{\rm Z}, m_{\rm H}) \tag{5}$$

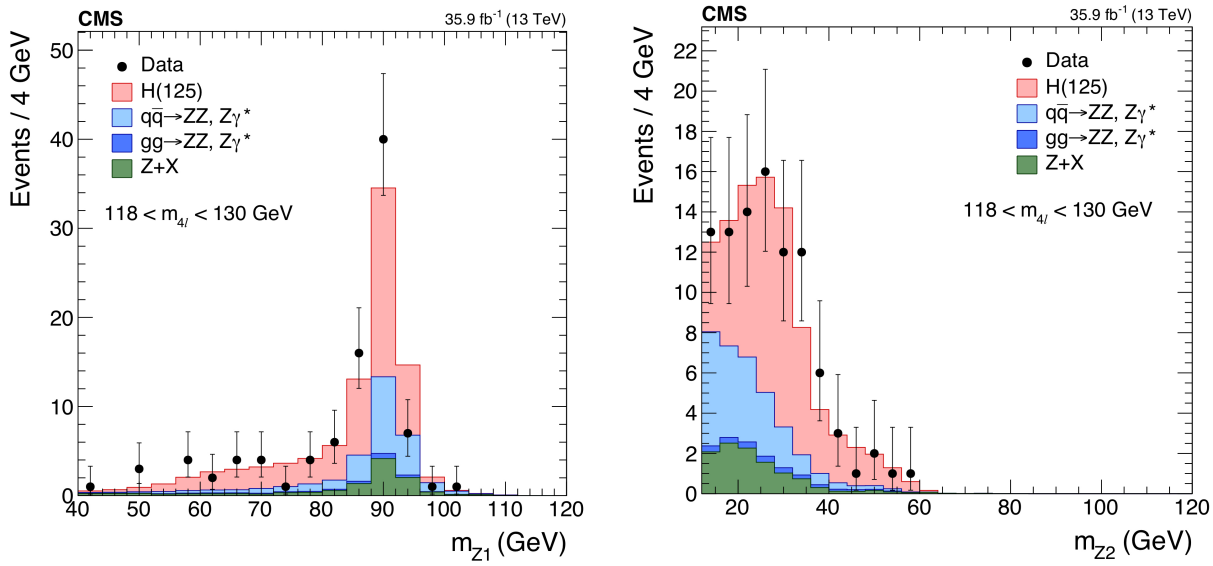

Figure 4: (Left) Invariant mass distribution of $Z \to \ell^-\ell^+$ events whose dilepton invariant mass is closer to the PDG value of the Z boson (91.188 GeV) than the other dilepton pair invariant mass. The Z_1 has a narrow width and is mostly on-shell. (Right) Invariant mass distribution of the dilepton events whose mass is farther from the Z boson PDG value as compared to the other dilepton pair. In both mass distributions, it is required that $118 < m_{4\ell} < 130$ GeV [4].

where p_T^1 and p_T^2 are the reconstructed p_T values of the two leptons originating from the Z_1, δp_T^1 and δp_T^2 are the corresponding per-event lepton p_T uncertainties, $\hat{p}_T^1$ and $\hat{p}_T^2$ are the refitted p_T values of the two leptons, and m_{12} is the invariant mass calculated using the refitted p_T values. Here, m_Z is set to the PDG value for the Z boson mass (91.188 GeV), m_H is set to 125 GeV corresponding to the mass use in simulated $H \to ZZ \to 4\ell$ events, and lastly the $\mathcal{L}(m_{12}|m_Z, m_H)$ is the mass constraint term on the $m(Z_1)$.

Per event, the likelihood given by Eq. 5 is maximized by the mass constraint term and the newly-obtained refitted lepton p_T values are used to update the first two observables $(m_{4\ell}, \mathcal{D}_{\text{mass}})$, which are then denoted by a prime ($'$):

$$m_{4\ell} \to m'_{4\ell}$$
$$\mathcal{D}_{\text{mass}} \to \mathcal{D}'_{\text{mass}}.$$

Using the $m(Z_1)$ mass constraint to obtain refitted lepton p_T values in this fashion provides greater precision on the final Higgs boson mass measurement, as shown in Fig. 5 [4].

4 Conclusions

The mass of the Higgs boson (m_H) was extracted by a three-dimensional likelihood fit using three observables: $m'_{4\ell}, \mathcal{D}'_{\text{mass}}, \mathcal{D}^{\text{kin}}_{\text{bkg}}$. The data used in this measurement were collected by the CMS detector corresponding to an integrated luminosity of 35.9 fb^{-1} from proton-proton collisions provided by the LHC during the 2016 Run. The Higgs boson mass was measured to be $m_H = 125.26 \pm 0.21$ (± 0.20[stat.] $\pm$ 0.08[sys.]) GeV, which achieved a better overall precision than the previous m_H measurement of 125.09 ± 0.24 (± 0.21[stat.] ± 0.11[sys.]) GeV, made by the ATLAS

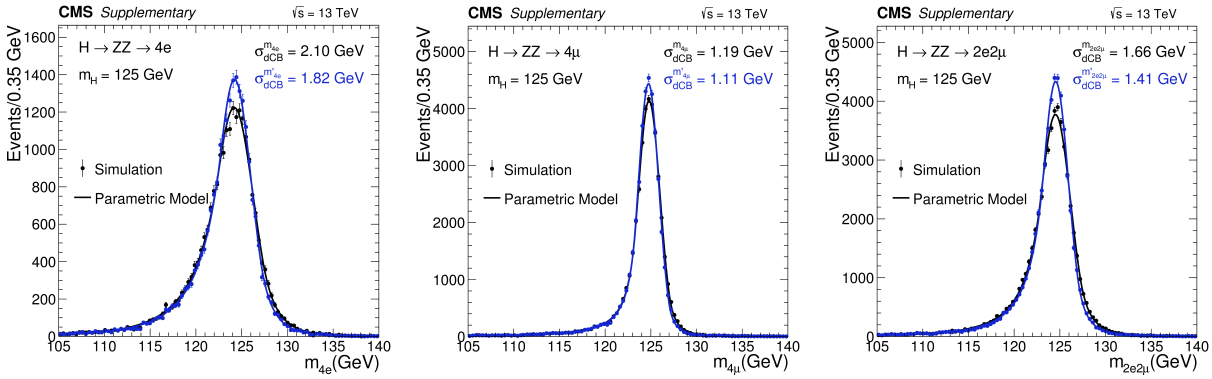

Figure 5: Distributions of the $m_{4\ell}$ in $\mathrm{H} \to \mathrm{ZZ} \to 4\ell$ events using reconstructed lepton p_{T} values (black line) and refitted p_{T} values (blue line), separated by each final state: 4e (Left), 4μ (Center), $2e2\mu$ (Right). The refitted distributions are obtained by imposing the mass constraint on the $m(\mathrm{Z}_1)$. Each curve is fit with a double Crystal Ball pdf and the resolution of the peak (σ_{dCB}) is extracted. The resolution improvement between reconstructed and refitted distributions is 7% in the 4μ channel, 13% in the $2e2\mu$ channel, and 15% in the 4e channel [4].

No $m(\mathrm{Z}_1)$ constraint	3D: $\mathcal{L}(m_{4\ell}, \mathcal{D}_{\mathrm{mass}}, \mathcal{D}^{\mathrm{kin}}_{\mathrm{bkg}})$	2D: $\mathcal{L}(m_{4\ell}, \mathcal{D}_{\mathrm{mass}})$	1D: $\mathcal{L}(m_{4\ell})$
Expected m_{H} uncertainty change	+8.1%	+11%	+21%
Observed m_{H} (GeV)	125.28±0.22	125.36±0.24	125.39±0.25
With $m(\mathrm{Z}_1)$ constraint	3D: $\mathcal{L}(m'_{4\ell}, \mathcal{D}'_{\mathrm{mass}}, \mathcal{D}^{\mathrm{kin}}_{\mathrm{bkg}})$	2D: $\mathcal{L}(m'_{4\ell}, \mathcal{D}'_{\mathrm{mass}})$	1D: $\mathcal{L}(m'_{4\ell})$
Expected m_{H} uncertainty change	—	+3.2%	+11%
Observed m_{H} (GeV)	125.26±0.21	125.30±0.21	125.34±0.23

Table 2: A summary of the precision gained by refitting the lepton p_{T} values which come from a mass constraint on the $m(\mathrm{Z}_1)$ (comparison across rows) and by introducing a 1D, 2D, or 3D fit likelihood fit (comparison across columns) using the observables described in Section 2. The greatest precision gain is observed when comparing a 1D likelihood fit (with no mass constraint) to a 3D fit (with a mass constraint) which results in a 21% gain in precision on the Higgs boson mass measurement [4].

and CMS Collaborations, which corresponded to an integrated luminosity of approximately 25 fb^{-1} per collaboration from LHC proton-proton collision data in 2010 and 2011. The 1D likelihood scan vs. m_{H} accounting for one, two, and three observables is shown in Fig. 6 (Left) and split up into different final states: 4e, 4μ, 2e2μ (Right) [4]. Finally, the precision gained by using 1D, 2D, and 3D likelihood fits, with and without a mass constraint on the $m(\mathrm{Z}_1)$, is given in Table 2 [4]. It should be noted that while these these proceedings were being written, an even more precise measurement of the Higgs boson mass was made public [10].

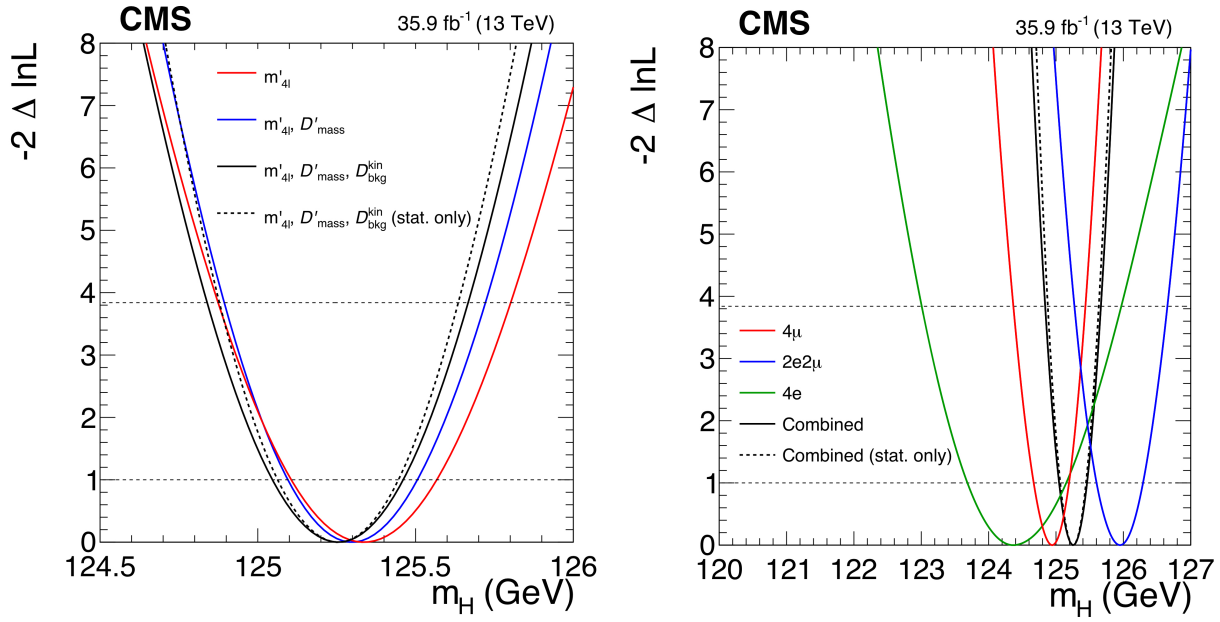

Figure 6: (Left) A likelihood scan of the Higgs boson mass using one (red), two (blue), or three (black) observables. The dashed black line includes only statistical uncertainty, whereas the solid black line includes both statistical and systematic uncertainty. (Right) The 1D likelihood scan is split up into the different final states: 4μ (green), 2e2μ (blue), and 4e (green). Again, the dashed black line includes only statistical uncertainty, whereas the solid black line includes both statistical and systematic uncertainty [4].

Acknowledgements

This work is presented on behalf of the CMS collaboration. The author is grateful to Prof. Andrey Korytov, for the opportunity to present at DPF, to Dr. Hualin Mei, for having developed the bulk of the analysis, and to Dr. Filippo Errico for his limitless patience.

References

[1] G. Aad *et al.* [ATLAS Collaboration], "Observation of a new particle in the search for the Standard Model Higgs boson with the ATLAS detector at the LHC," Phys. Lett. B **716**, 1 (2012) doi:10.1016/j.physletb.2012.08.020 [arXiv:1207.7214 [hep-ex]].

[2] S. Chatrchyan *et al.* [CMS Collaboration], "Observation of a New Boson at a Mass of 125 GeV with the CMS Experiment at the LHC," Phys. Lett. B **716**, 30 (2012) doi:10.1016/j.physletb.2012.08.021 [arXiv:1207.7235 [hep-ex]].

[3] G. Aad *et al.* [ATLAS and CMS Collaborations], "Combined Measurement of the Higgs Boson Mass in *pp* Collisions at $\sqrt{s} = 7$ and 8 TeV with the ATLAS and CMS Experiments," Phys. Rev. Lett. **114**, 191803 (2015) doi:10.1103/PhysRevLett.114.191803 [arXiv:1503.07589 [hep-ex]].

[4] A. M. Sirunyan *et al.* [CMS Collaboration], "Measurements of properties of the Higgs boson decaying into the four-lepton final state in pp collisions at $\sqrt{s} = 13$ TeV," JHEP **1711**, 047 (2017) doi:10.1007/JHEP11(2017)047 [arXiv:1706.09936 [hep-ex]].

[5] S. Chatrchyan *et al.* [CMS Collaboration], "The CMS Experiment at the CERN LHC," JINST **3**, S08004 (2008). doi:10.1088/1748-0221/3/08/S08004

[6] Y. Gao, A. V. Gritsan, Z. Guo, K. Melnikov, M. Schulze and N. V. Tran, "Spin Determination of Single-Produced Resonances at Hadron Colliders," Phys. Rev. D **81**, 075022 (2010) doi:10.1103/PhysRevD.81.075022 [arXiv:1001.3396 [hep-ph]].

[7] S. Bolognesi, Y. Gao, A. V. Gritsan, K. Melnikov, M. Schulze, N. V. Tran and A. Whitbeck, "On the spin and parity of a single-produced resonance at the LHC," Phys. Rev. D **86**, 095031 (2012) doi:10.1103/PhysRevD.86.095031 [arXiv:1208.4018 [hep-ph]].

[8] I. Anderson *et al.*, "Constraining Anomalous HVV Interactions at Proton and Lepton Colliders," Phys. Rev. D **89**, no. 3, 035007 (2014) doi:10.1103/PhysRevD.89.035007 [arXiv:1309.4819 [hep-ph]].

[9] S. Choudhury, "Measurements of the Higgs Boson at the LHC and Tevatron," EPJ Web Conf. **90**, 05002 (2015). doi:10.1051/epjconf/20159005002

[10] CMS Collaboration, CMS-PAS-HIG-19-004 (2019) url:https://cds.cern.ch/record/2691211